

Metal Nanoparticles

Synthesis, Characterization, and Applications

edited by

Daniel L. Feldheim

North Carolina State University, Raleigh, North Carolina

Colby A. Foss, Jr.

Georgetown University, Washington, D.C.



MARCEL DEKKER, INC.

NEW YORK • BASEL

6

Nonlinear Optical Properties of Metal Nanoparticles

Robert C. Johnson and Joseph T. Hupp
Northwestern University, Evanston, Illinois

I. INTRODUCTION AND BACKGROUND

Nonlinear optics (NLO) is an interesting and active field of research and development where activity is now largely driven by a desire to progress toward real-world applications of novel technologies (1). A compelling emerging application of nonlinear optics is photonics, the photon-based analog of electronics, which utilizes nonlinear phenomena (e.g., sum- and difference-frequency generation and frequency doubling) for predictable modification, translation, and switching of optical signals. The fundamental physical principles of nonlinear photonics are well established. The challenge comes in discovering and/or designing materials that satisfy the technological requirements accompanying both proof-of-concept device demonstrations and practical applications. From this perspective, nonlinear photonics is an exceptionally multidisciplinary field, engendering the interest and efforts of engineers, chemists, physicists, and materials scientists. Eventual applications must successfully integrate fundamental (shedding light on the mechanisms of NLO response and enhancement) and applications-based (device design and materials synthesis) work. Accordingly, much of the chemical research in nonlinear optics and photonics has centered on development of new molecules, polymers, and other materials with favorable and programmable NLO properties. Almost all commercially available NLO devices, however, are still based on simple inorganic crystals such as potassium dihydrogen phosphate (KTP); such crystals are widely used, for example, as frequency doublers in laser applications. Nevertheless, organic molecules and polymers are potentially highly attractive for NLO purposes, offering superior mechanical properties, structural

and physical tailorability, and a potentially wider range of optical properties. As the wealth of synthetic knowledge has grown, the search for novel, potent NLO materials has become correspondingly sophisticated and exotic.

Despite their remarkable optical properties, and though their existence has been known for nearly a century and a half, metal nanoparticles have not been included in this search until recently. While the linear optical properties of metal nanoparticles have been extensively investigated, the potential of these materials for nonlinear optical applications has been largely untapped. Nevertheless, because superior NLO responsivity is largely a matter of attaining superior electronic polarizability and hyperpolarizability (see below), one might expect metal nanoparticles, with their exceptionally high density of delocalized electrons, to be good-candidate NLO materials. This chapter summarizes recent studies of the nonlinear optical properties of metal nanoparticle solutions and suggests applications beyond the general goals of NLO research. While supported metal nanoparticles or nanoparticle films have been by comparison well investigated in this regard, these topics are not included here. Brief introductions to NLO and relevant experimental techniques are provided; the interested reader may consult the references for a more technical analysis.

II. NLO: THEORETICAL BACKGROUND

The effectiveness of NLO chromophores can be quantified and compared by tabulating NLO properties which describe the magnitude of the nonlinear response. Briefly, an intense electromagnetic field interacting with matter induces within the matter a dipole P_{ind} that can be expressed as

$$P_{\text{ind}} = \alpha_{ij} E_j + \beta_{ijk} E_j E_k + \gamma_{ijkl} E_j E_k E_l + \dots \quad (1)$$

The subscripts represent the molecular or particle coordinates x, y, z ; repeated subscripts indicate summation over the three components. E_j is the electric field component along the j axis. α, β , and γ represent the polarizability, first hyperpolarizability, and second hyperpolarizability tensors, respectively. α describes the linear response to the field, while β, γ , etc., describe the nonlinear response. β is the quantity in which the second-order response is manifested; from a chemical perspective, maximizing β is a primary objective. For dipolar molecules β is generally dominated by the component β_{zzz} , where z is the axis aligned with the molecular dipole. More detailed discussions about β are given elsewhere (2–4).

Perhaps the most common NLO phenomenon is second-harmonic generation (SHG), which is coherent light scattering at double the incident frequency. As with all even-order nonlinear optical processes, SHG is to a first approximation absent for species featuring a center of symmetry (5). SHG is also absent for collections of species when the species are configured such that signals (vector

quantities) from individual moieties cancel each other. This includes, to a very good approximation, isotropic solutions of chromophores which individually are capable of SHG. [An important exception has been described by Eisenthal and co-workers, who showed that residual coherent SHG can be obtained from solutions which are macroscopically centrosymmetric but contain organized, ordered, and locally noncentrosymmetric chromophoric domains having dimensions comparable to, or in some cases even as small as ca. 10%, of the wavelength of incident light (6).]

Solution SHG measurements can be made via the EFISHG (electric-field-induced second-harmonic generation) technique, in which an external electric field is applied to orient dipolar solute molecules. Briefly, the orientation breaks the overall centrosymmetry of the solution, thereby permitting generation of a second-order signal. From a slightly different perspective, the sensitivity of SHG to symmetry reduction has been very effectively exploited by surface scientists, who have recognized that interface formation necessarily causes a loss of centrosymmetry. SHG can be used, therefore, as an interface-specific structural and analytical tool (7). Although this interesting field is beyond the scope of this chapter, a handful of studies of coherent SHG are described, including one involving a nanoparticle film which bears relevance to this chapter.

While coherent SHG is the preferred method for NLO analysis of films and interfaces, a more effective technique for solution species is hyper-Rayleigh scattering (HRS), which is incoherently scattered second-harmonic light (essentially "incoherent SHG"). While HRS was experimentally demonstrated in 1965 (8), not until decades later did it become popular as a means for obtaining first hyperpolarizabilities for solution species (9). At first glance, HRS would appear to be impossible: nonlinear scattering, for example, from dipolar molecules comprising a truly isotropic solution should lead to overall cancellation and no net signal. To a large extent this is true: HRS signals are typically several orders of magnitude less intense than coherent SHG signals from the same nonlinear chromophores because the doubling signals from individual, randomly oriented chromophores indeed do nearly completely cancel each other. Briefly, HRS works, despite the orientational randomization, because signals scale as the variance of the orientation of the chromophoric species with respect to the electromagnetic field (10). (Thus, although orientational randomization necessarily results in an average electromagnetic polarization of zero, the variance of the orientation is nonzero.) HRS also circumvents the need to orient the scattering entities within the sample and can thus be used to analyze, for example, solutions of ionic and nondipolar species, both of which are inaccessible to SHG experiments.

In general, the experimental hyper-Rayleigh scattered intensity ($I_{2\omega}$) is given by

$$I_{2\omega} = G \times B^2 \times (I_\omega)^2 \times \exp(-N_c \sigma_{c(2\omega)} l) \quad (2)$$

where B is the (macroscopic) second-order susceptibility. For a two-component (solute plus solvent) solution, B^2 is

$$B^2 = \langle N_c \beta_c^2 + N_s \beta_s^2 \rangle \quad (3)$$

where the brackets indicate an average over all chromophore orientations. Subscripts c and s denote chromophore and solvent, respectively; G contains instrumental factors, collection efficiency, and local field factors; N represents concentration; I_ω is the intensity of the incident fundamental light; $\sigma_{c(2\omega)}$ is the absorption cross section at the second-harmonic wavelength; and l is the effective scattering pathlength. The exponential term accounts for self-absorption of the scattered photons.

Details of HRS setups and experimental procedures are provided elsewhere (10,11). The HRS signal is very weak, so a high-power laser source and appropriately sensitive detection are necessary. Depending on the wavelength of interest, typically the output of a nanosecond-pulsed Nd:YAG laser (1064 nm), a Nd:YAG-pumped optical parametric oscillator (broadly tunable within the visible and near-infrared spectral regions), or a femtosecond-pulsed titanium-sapphire laser (typically tunable from ca. 720–1100 nm) is used. If the solvent's β is known at the relevant wavelength, the HRS measurements can be internally referenced against the solvent. Alternatively, a different chromophore with a known β at the wavelength of interest can be used as an external reference. Since β_c usually exceeds β_s by a few to several orders of magnitude, the external reference method is typically less sensitive to small uncertainties in measurement and is thus inherently more accurate.

Several components of the β tensor can be extracted by performing second-order light-scattering experiments using incident fundamental frequencies ω_1 and ω_2 (for HRS experiments, $\omega_1 = \omega_2$) and intelligently choosing the polarizations of the incident and scattered light (12). One simple yet informative experimental variation of HRS is the measurement of D , the ratio of the intensities of vertically polarized and horizontally polarized HRS signals obtained by using vertically polarized incident light. D , which is approximately equal to β_{zzz}/β_{xxx} , can provide symmetry information when molecular scatterers are involved. For example, $D = 5.0$ for molecules with C_{2v} symmetry and $D = 1.5$ for purely octupolar species (13). Depolarization experiments on metal nanoparticles are described below.

III. GOLD, SILVER, AND COPPER NANOPARTICLES

Although theories of nonlinear scattering from metal nanoparticles are discussed later, a simplified treatment of the corresponding theory for *molecular* chromophores is summarized in Eq. (4), which is applicable to a hypothetical system characterized by a ground electronic state and a single charge-transfer excited


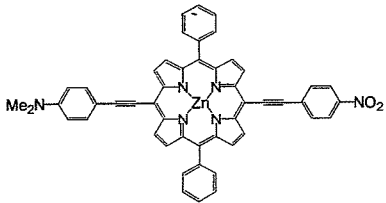
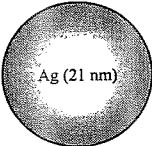

state (denoted as 1 and 2, respectively), and an infinitely narrow charge transfer absorption band (14):

$$\beta = \frac{3\mu_{12}^2 \Delta \mu_{12} E_{op}^2}{2(E_{op}^2 - E_{inc}^2)(E_{op}^2 - (2E_{inc})^2)} \quad (4)$$

In the equation, μ_{12} is the transition dipole moment—a quantity closely related to the absorption intensity or oscillator strength, $\Delta \mu_{12}$ is the change in dipole moment upon optical excitation (proportional to the degree and distance of internal charge transfer accompanying excited-state formation), and E_{op} and E_{inc} are the energies of the optical transition and the incident light, respectively. This model predicts signal enhancements at wavelengths that are one- or two-photon resonant with an optical transition. It also predicts large signals for strongly allowed electronic transitions.

We and others reasoned that gold nanoparticles, with their spectacularly intense visible-region absorption bands (collective electron excitation or “plasmon” bands), might prove particularly effective as nonlinear optical chromophores. In HRS studies by Vance and co-workers with 13-nm, citrate-stabilized gold particles in aqueous solutions, an enormous hyperpolarizability— 7×10^{-25} esu—was recorded with $E_{inc} = 12,200 \text{ cm}^{-1} = 1/(820 \text{ nm})$ (15). Similarly large hyperpolarizabilities have recently been reported by Galletto and co-workers (17). For comparison, β for the standard NLO benchmark compound, *p*-nitroaniline, is 34×10^{-30} esu at 1064 nm, while for water it is 0.56×10^{-30} esu. The comparison, of course, is somewhat misleading because a single gold nanoparticle contains thousands of atoms, while most molecular chromophores contain less than a hundred. Clearly, some sort of normalization is required in order to make meaningful comparisons. For photonic applications, perhaps the best figure of merit is β^2 per unit volume. (Recall that NLO responses scale as β^2 rather than β . If the candidate nonlinear chromophores are dipolar and are ultimately used in ways that require the application of an external field in order to attain alignment, and, therefore, net signal generation, then the most meaningful figures of merit could also include the dipole moment.) A slightly more convenient figure of merit—one which obviates the need to consider packing differences, bond-length differences, etc.—is β^2 per atom. As shown in Table 1, the normalized nonlinear scattering efficiency of the gold nanoparticle sample (partially resonant) exceeds by several orders of magnitude the off-resonance efficiencies of the best existing molecular NLO chromophores. In the molecular NLO chromophore literature, responses are typically reported in terms of β rather than β^2 ; therefore, Table 1 also includes $(\beta^2/\text{atom})^{1/2}$. For either figure of merit, it remains to be seen how great the nanoparticle/molecule disparity is under conditions where both sets of measurements are made off resonance; almost certainly, however, the disparity will be less.

Table 1

Scatterer	β (10^{-30} esu)	β^2/atom (10^{-60} esu)	$(\beta^2/\text{atom})^{1/2}$ (10^{-30} esu)
H ₂ O	0.56 ^a	0.10	0.32
	34 ^b	72	8.5
	5000 ^{a,c}	2.7×10^5	520
	7×10^5 ^{b,d}	7×10^5	840
	7×10^5 ^{a,e}	8×10^6	2800

^a 820-nm incident radiation.^b 1064-nm incident radiation.^c From Ref. 16.^d From Ref. 20.^e From Ref. 15.

What about nanoparticle size effects? At some point, as the size of the nanoparticle is increased, one would expect to see primarily residual coherent SHG, rather than HRS, thereby complicating the extraction of β^2 from the observed doubled-light intensities. Fortunately, there is a simple experimental diagnostic for distinguishing residual coherent SHG from HRS: signals for the former

scale with the square of the chromophore concentration, while signals for the latter scale linearly. In any case, Galletto and co-workers have reported on size effects over the 5- to 22-nm-diameter particle range, using incident light at 1064 nm (17). Using β/atom as a figure of merit, they reported striking decreases in HRS response with increasing particle size. By using what we would argue is a more meaningful figure of merit, β^2/atom , the available data actually point to a significant *increase* in normalized efficiency with increasing particle size (Fig. 1). Notably over the same size range (a) the linear absorptivity, and therefore μ_{12} [see Eq. (4)], remain more or less constant on a per atom basis, and (b) the plasmon absorption maximum moves from 508 to 520 nm when the particle diameter is changed from 5 to 22 nm, perhaps slightly changing resonance effects.

What about wavelength effects? Qualitatively for 13-nm gold particles we find that nonlinear scattering occurs more efficiently with excitation at 1064 nm than at 820, 760, or 720 nm. This would be consistent with a two-photon enhancement effect due to resonance with a plasmon absorption band near 532 nm. More compelling evidence for plasmon resonance enhancement comes from closely related SHG measurements: excitation profiles for colloidal gold particles at the air-toluene interface, using a range of second-harmonic wavelengths tuned to include the plasmon absorption, show a narrow peak in the SHG profile centered near the absorption peak (18). Nanoparticles embedded in alumina and deposited

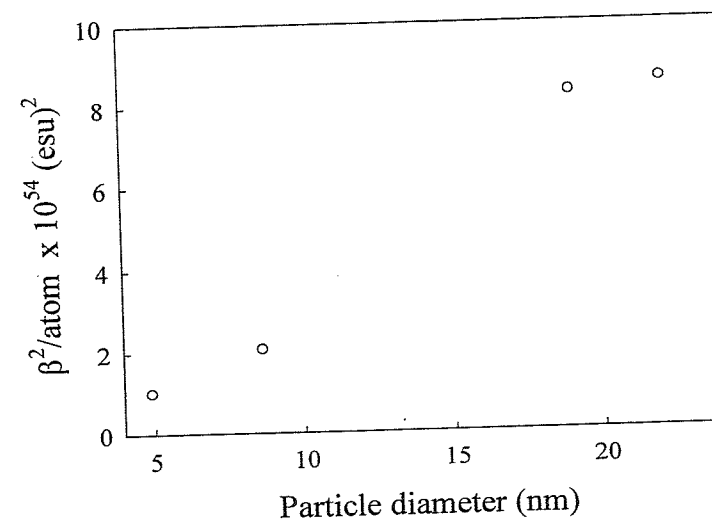


Fig. 1. Relative HRS response of gold nanoparticles of varying size; based on data from Ref. 17.

on silica behave similarly: the SHG excitation profile shows a peak centered near the plasmon absorption maximum (19). The combined experiments additionally show that nonlinear spectroscopic response also depends on the surrounding medium, at least in an energetic sense: the position of the plasmon peak for the supported particles is red-shifted compared to the solution particle (see Chapter I), and the SHG excitation profile is similarly red-shifted.

Can the phenomenon be observed with metal nanoparticles other than gold? The first reports of HRS from metal nanoparticles were for silver, not gold (20,21). Triest and co-workers reported seemingly modest HRS signals from colloidal silver nanoparticle suspensions: $\beta/\text{atom} \approx (0.7 \text{ to } 1.0) \times 10^{-30}$ esu, where the variability reflects differences in particle size. If the results are recast as $(\beta^2/\text{atom})^{1/2}$, the responses are rather more impressive: ca. 800×10^{-30} esu for the smallest particles examined (cf. Table 1). Notably, the particles examined by these investigators featured a narrow plasmon absorption centered at 400 nm and, therefore, exhibited absorbance at neither the fundamental (1064 nm) nor the second-harmonic (532 nm) wavelength of the experiment. Unpublished studies at Northwestern, based on wavelength-tunable excitation, reveal a strong two-photon enhancement effect due to plasmon resonance, with resonant $(\beta^2/\text{atom})^{1/2}$ values as large as $\sim 7000 \times 10^{-30}$ esu (22).

Further studies using 820-nm incident light show that copper nanoparticles also are capable of strong nonlinear responses, comparable to those of silver and gold (22). Presumably the strong response is due to partial plasmon resonance in both one- and two-photon senses. The copper particle spheres interrogated by HRS spectroscopy featured a broad, but intense, plasmon absorption band centered at ~ 560 nm. In contrast, similarly sized tetrahedral platinum particles yielded no detectable hyper-Rayleigh scattering. The key difference between platinum and the coinage metals is presumably the absence of a visible-region plasmon band, needed for resonance enhancement.

IV. AGGREGATION EXPERIMENTS

The incoherent second-harmonic response from gold colloids is enhanced upon coagulation of the nominally spherical particles into larger random (and presumably nonspherical) aggregates. This has been shown by HRS experiments on gold with aggregation induced by addition of salt (15) or pyridine (23). Aggregation causes broadening of the plasmon peak and increases in extinction at longer wavelengths (600–800 nm). Under conditions of extreme aggregation the original plasmon absorption peak disappears essentially completely (Fig. 2). In view of the prime role played by the plasmon absorption in enhancing the particles' nonlinear optical response, it is tempting to conclude that the further enhancement accompanying aggregation is a consequence of plasmon band energy shifts and a

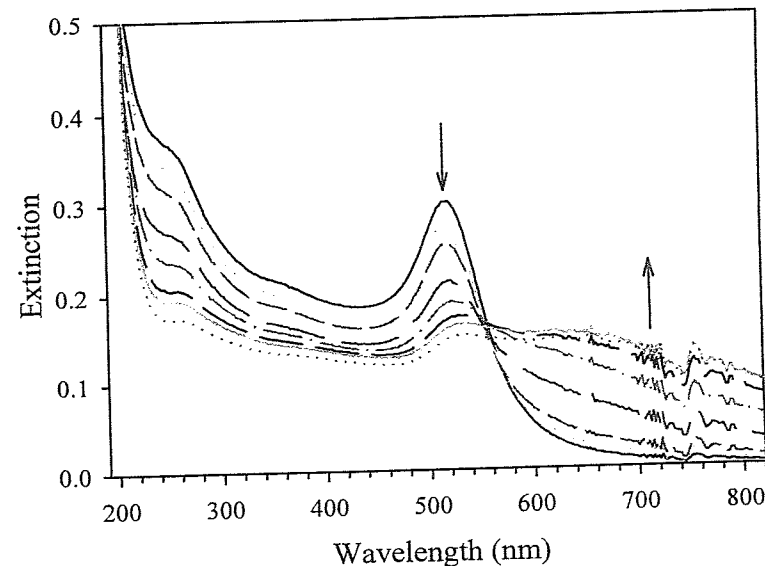


Fig. 2. UV-vis extinction spectra recorded after successive additions of 6.0 M NaCl to a solution of 13-nm gold nanoparticles (15). (Reproduced with permission from J. Phys. Chem. B., 1998, 102, 10091–10093. Copyright 1998 Am. Chem. Soc.)

resulting improvement in optical resonance. A more careful evaluation shows, however, that the large increase in HRS response occurs before the aggregation process has progressed far enough to cause noticeable changes in the linear extinction spectrum (15). Instead, HRS signal enhancement appears to be associated with small aggregate formation, with further aggregation having little additional effect. This is shown in a striking way in Fig. 3, from Vance and co-workers, where the linear scattering response (Rayleigh scattering, a rough measure of aggregate size) is plotted together with the second-order scattering response (hyper-Rayleigh response) as a function of the amount of aggregation agent added: HRS is clearly more sensitive to the formation of small aggregates than is Rayleigh scattering.

Why does the otherwise inconsequential formation of very small aggregates lead to such extensive enhancement of the metal nanoparticles' nonlinear scattering capabilities? Recall that the available *molecular* theory precludes dipole-based frequency doubling by centrosymmetric chromophores, such as spherical nanoparticles. If a particle aggregate behaves electromagnetically as a single collective chromophore rather than a collection of individual chromophores, then the overall symmetry and not just the symmetry of the component particles comes into play. Evidently, small aggregate formation causes a sufficient decrease in

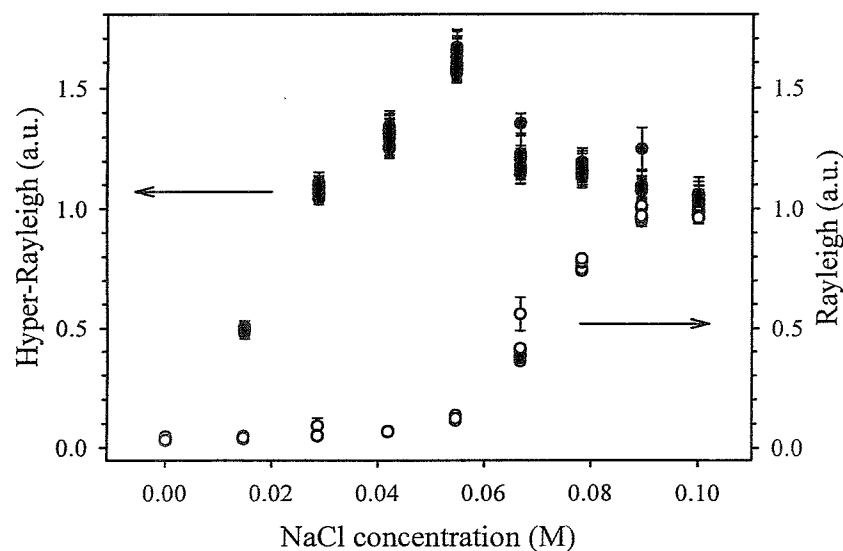


Fig. 3. Comparison of Rayleigh (open circles) and hyper-Rayleigh (filled circles) signals from 13-nm gold nanoparticles after aggregation induced by addition of 6.0 M NaCl solution (15).

collective symmetry (centrosymmetry) to permit the observation of an additional NLO response that would otherwise be cancelled. Furthermore, the reduction in chromophoric centrosymmetry upon small aggregate formation is sufficiently great that further aggregation, and further symmetry reduction, offer no additional advantage.

Although shifts in plasmon band energy and intensity appear not to play a dominant role in the studies of salt-induced aggregation summarized in Figs. 2 and 3, these effects might be important under other conditions (other excitation wavelengths, other aggregation agents, etc.) The formation of ellipsoidal aggregates rather than highly asymmetric aggregates has been observed for pyridine-induced aggregation (24). Note that a *perfect* ellipsoid, like a perfect sphere, possesses an inversion center and therefore should offer no advantage in a nonlinear scattering experiment. In any case, gold nanoparticle aggregates of approximately spheroidal shape display a substantially enhanced HRS response (23). They also display a broad extinction in the near IR not seen for the component spherical particles; this feature has been assigned as a longitudinal plasmon absorbance attributable to an electromagnetic response of each of the aggregates as a whole. (The precise shape and location of the longitudinal band depend on aggregate size and

aspect ratio.) In any case, as Galletto and co-workers have noted, the enhancement in HRS upon formation of these aggregates might well be due to partial resonance of this new band with the 1064-nm incident radiation used in these experiments (23). Excitation profiles could prove helpful in establishing the extent to which longitudinal resonance effects are responsible for the HRS enhancement phenomenon. When coupled with available theory for deconvolving the linear extinction spectrum (25), the profiles should prove helpful in determining to what extent scattering versus absorption can contribute to HRS resonance effects. As one would expect, longitudinal plasmon resonance effects also are very much in evidence in the linear extinction spectra of rod-shaped gold particles. Templated synthesis of such particles with precise control over the particle dimensions has been reported (26,27), but no nonlinear optical experiments of suspensions of these interesting particles have yet been reported. Coherent SHG from aligned arrays of rod-shaped gold particles, however, has recently been reported (28).

The possible existence of yet another set of HRS enhancement schemes has been suggested by Triest and co-workers (20,21). They found, with silver nanoparticles, that adsorption of *p*-nitroaniline—itsself a nonlinear chromophore—greatly increases the NLO response. They suggested that this could be the result of (a) a collective response from aligned dye molecules at the particle surface, (b) electromagnetic enhancement by the nanoparticle of the *molecular* chromophore's HRS response, perhaps in a fashion reminiscent of known mechanisms for surface-enhanced Raman scattering (29), or (c) fortuitous resonance with particle-dye charge-transfer transitions. (The authors also discussed the possibility of enhancement due simply to dye-adsorption-induced aggregation.) Mechanism (c) has an interesting precedent in studies by Liu and co-workers of residual coherent SHG from catechol-functionalized semiconductor particles (30). For mechanism (b) a combination of polarization and excitation-profile studies might be sufficient to establish the degree of applicability to the silver/*p*-nitroaniline system.

In the same study (20), these authors also reported that, in the absence of a chromophoric adsorbate, the normalized nonlinear scattering efficiency, expressed as β/atom , systematically increases with increasing particle diameter; over the admittedly limited size range examined (26–34 nm), the normalized HRS response appears to scale linearly with diameter. If the findings are recast in terms of β^2/atom (see above), the normalized dependence of the nonlinear scattering efficiency upon particle size of course becomes stronger.

V. CORE-SHELL PARTICLES

Core-shell nanoparticles are becoming increasingly popular due to their interesting electronic properties. The shell provides an extra size variable and allows for tunability of the composite particle properties. The syntheses of such particles

have recently received increasing attention, and their linear optical properties have been addressed and correlated with theoretical prediction (25,31). However, the NLO properties of core-shell particles have not, to our knowledge, been seriously investigated. Recall that the visible-region optical properties of small-particle gold and silver colloids arise mainly from plasmon resonance effects, which in turn depend on polarization resonance effects whose energies are determined by dielectric functions for both the particles and their surroundings. One might expect the environmental dielectric modification associated with shell formation to have some impact, therefore, on the NLO properties of the colloids.

Preliminary HRS experiments on solutions of 13-nm gold core particles encased in a thin (4 nm) shell of silica show a collective signal roughly five times smaller than that of the unencapsulated particles (32). It should be noted that colloidal silica also exhibits a sizable HRS signal [$(\beta^2/\text{SiO}_2 \text{ unit})^{1/2} = 60\text{--}250 \times 10^{-30}$ esu for 10-nm colloidal particles (33)]; presumably the silica shell provides some of the HRS signal from the core-shell particles as well. Preliminary HRS depolarization ratio measurements (see NLO background section) yield a D value of 3.7 ± 0.4 for the silica-coated gold particles. While this does not approach the extremely large value reported for colloidal silica ($D_{\text{silica}} = 22 \pm 3$) (33), it is clearly larger than that of naked gold particles ($D_{\text{gold}} = 2.2 \pm 0.3$; see Fig. 4) (15), suggesting that the silica shell is indeed playing some role in the nonlinear scattering response of the composite species. The D values should not be interpreted as providing symmetry information about the particles; rather, they serve as a qualitative indicator that both core and shell components may be contributing to the observed HRS signal.

Why does shell formation have such a significant effect upon the nonlinear scattering efficiency? Despite the initial suggestion regarding electrostatic medium effects, the silica shells used in the preliminary HRS studies were too thin and perhaps too porous to alter the linear extinction spectrum. (Thicker shells, on the other hand, do induce the expected plasmon band red-shift and broadening.) A more prosaic explanation is that, under the conditions of the experiment, the silica shell prevents the gold particles from coalescing and hence eliminates intense HRS from residual low-symmetry aggregates otherwise present in the nominally nonaggregated sample. If the explanation is correct, then it indicates that the HRS signal enhancement accompanying aggregation and overall symmetry reduction is even greater than suggested above (i.e., ca. 40- to 50-fold rather than 8- to 10-fold).

While the silica shell provides protection against unintentional particle collision and aggregation, the core-shell particles can also be intentionally aggregated by addition of a difunctional linker ligand such as HBPA (hexane-1,6-bisphosphoric acid) (32). Preliminary work shows that when the acid groups bind the silica shells and cross-link the particles, they induce the familiar aggregation and color change. Linking also induces a substantial enhancement in the HRS response, showing that the aggregated nanoparticles can behave as collective low-

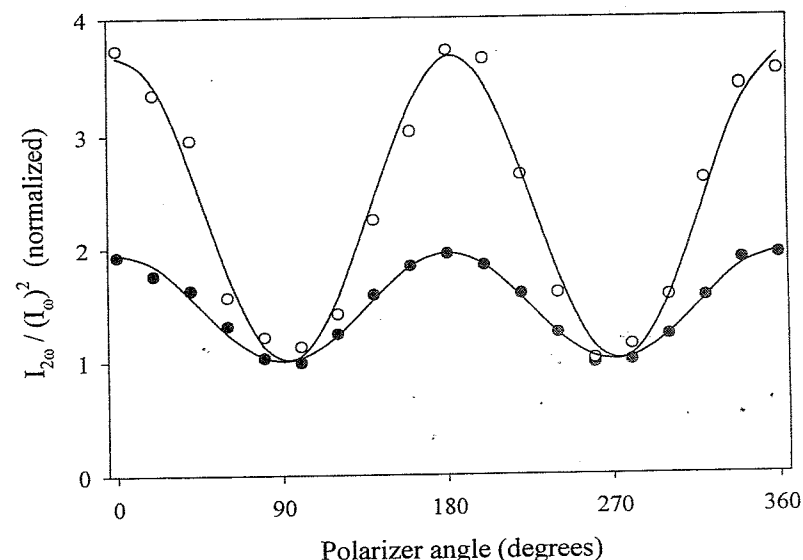


Fig. 4. Representative HRS depolarization experiments for naked 13-nm gold nanoparticles (filled circles, $D = 2.2 \pm 0.2$) and silica-coated 13-nm gold nanoparticles (open circles, $D = 3.7 \pm 0.4$). The curves are least-squares best fits of the data to $y = a \cos^2(x - c) + b$; the depolarization ratio D is equal to $(a + b) / b$. Both plots are normalized to signal = 1 at 90° .

symmetry chromophores despite physical separation (ca. 9 nm in this instance) due to the shell structures. The combined linear and nonlinear optical results also underscore a well-established but important characteristic of metal nanoparticles as chromophores. In comparison to molecular chromophores, metal particles display remarkably-long-range electromagnetic communication. Given the ready synthetic accessibility of core and shell structures of a variety of dimensions, further studies of the linear and nonlinear studies of these interesting composite particles and their aggregates could provide excellent tests of available theories regarding the distance dependence of particle-particle electromagnetic communication.

VI. DIMERS AND TRIMERS

While formation of random low-symmetry aggregates of colloidal metal particles clearly increases the incoherent second-harmonic response, a more detailed understanding can, in principle, be obtained by studying smaller aggregates of

particles with known symmetry. Brousseau and co-workers have shown that appropriately designed, rigid organic linkers can be used as templates for assembling nanoparticles into well-defined clusters (34). Prototypical examples of templated dimers and trimers of gold nanoparticles are shown in Fig. 5. From the perspective of nonlinear optical behavior, the important differences between the various trimers, dimers, and free monomers are symmetry and interparticle separation. For assemblies of identically sized particles, trimers are the smallest aggregates that lack a center of symmetry. Furthermore, for the trigonally arranged trimers in Fig. 5, the component metal particles are characterized by a much smaller average separation distance than in the corresponding dimer structures (see figure caption). Among the questions addressable with these and related aggregates are the following: (1) Can the NLO response of metal nanoparticles be influenced by symmetry over dimensions approaching those of the particles themselves? (2) Over what interparticle separation distances in solution can metal nanoparticles communicate electromagnetically?

Available linear extinction spectra show only slight differences between monomeric, dimeric, and trimeric species. Preliminary nonlinear experiments (820- or 1064-nm excitation), on the other hand, show small HRS signal enhancements upon dimer formation and large enhancements upon trimer formation, with the largest enhancement accompanying the formation of the more compact trimer (35). The preliminary experiments provide further evidence for the roles of both symmetry reduction and chromophore proximity in magnifying nonlinear optical responses from metal nanoparticle aggregates. Polarized HRS excitation/detection measurements point to a further behavioral difference between trimers, on the one hand, and dimers and monomers, on the other. For both trimers, the depolarization ratio is 1.5 ± 0.1 ; for the dimers and monomers it is ca. 2.2. The nominally trigonal planar geometry of the trimers* is reminiscent of molecular NLO chromophores also possessing D_{3h} symmetry (e.g., crystal violet). The molecular species lack the ground-state dipole moment usually required for second-order nonlinear behavior, but overcome this deficit by utilizing a molecular octupolar moment (36). A key experimental signature for molecular octupolar scatterers is a D value of 1.5. It is tempting to interpret the values for the trimeric metal particles as also indicating a role for octupolar moments, although appropriate theory to support or refute the interpretation has yet to be reported. Clearly, however, the depolarization ratio is a diagnostic feature that merits further consideration by theorists (43).

*Note that all assumptions about symmetry in dealing with metal nanoparticles are necessarily approximations. The particles are crystalline, and the faceted surface structure reduces the precise symmetry. Such effects are presumed to be negligible on the bulk scale.

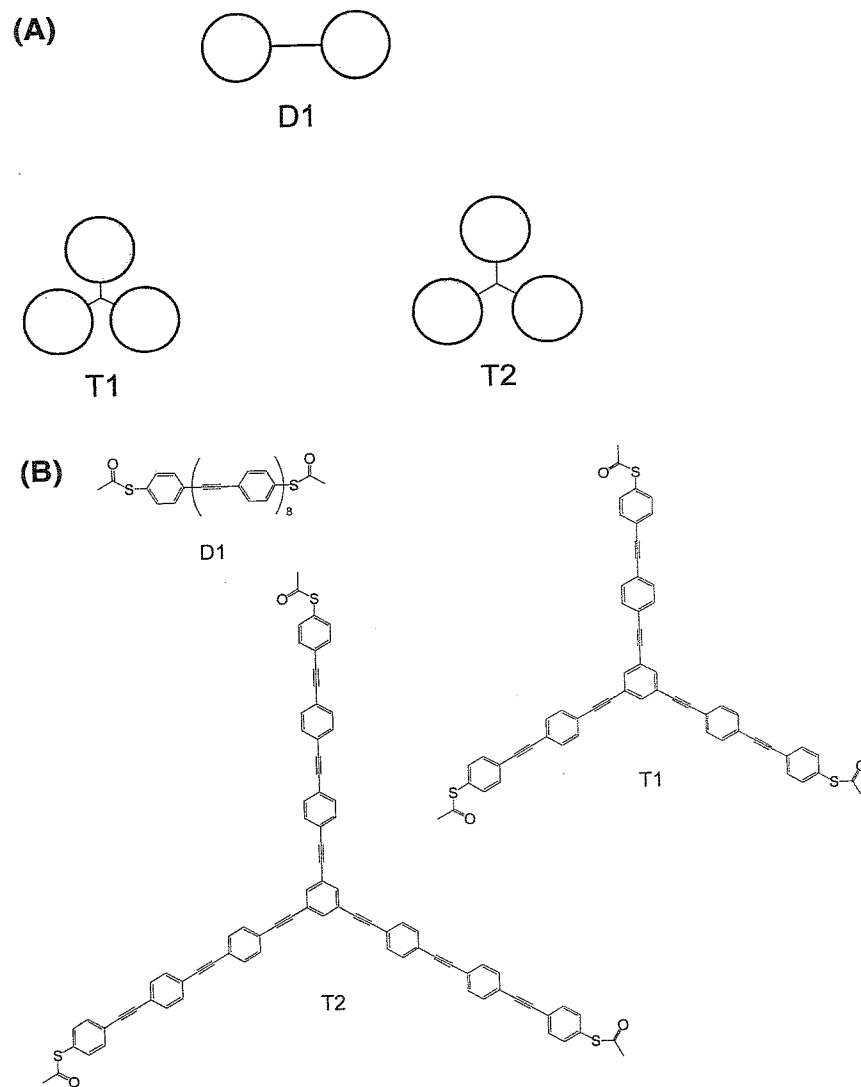


Fig. 5. (A) Schematic representation (drawn to scale) of organically linked dimer and trimers of 8-nm gold nanoparticles. Average interparticle spacings (surface to surface) for linked 8-nm-diameter spherical particles: (D1) 6.0 nm; (T1) 2.1 nm; (T2) 3.2 nm. (B) Chemical structures of the dimer and trimer linkers (34).

VII. LANGMUIR FILMS

An important non-solution-phase (or partial solution-phase) result that is relevant here has been reported by Collier et al. (37,38) The SHG response of Langmuir monolayers of small (≤ 4 nm) organic-ligand-capped silver nanoparticles to 1064-nm incident light was recorded continuously as the monolayers were compressed. The authors found that the change in susceptibility $\Delta\chi^{(2)}$ upon film compression displayed an exponential dependence upon average interparticle separation, indicative of distance modulation of particle-particle communication. The SHG signal was observed to increase sharply upon film compression, but with peaking followed by a dramatic falloff well before compression-induced collapse of the monolayer. The sharp decrease, seen for monolayers of 2.7-nm as well as 4-nm particles, was attributed to an insulator-to-metal transition within the monolayer. This interpretation was supported by linear reflectance data. As the authors note, these observations are an excellent example of the utility of SHG as a monitor of interparticle coupling.

VIII. THEORY

Second-harmonic generation from small metal particles was first investigated theoretically nearly two decades ago by Agarwal and Jha (39), before most of the experimental work on the subject had been performed. Enhancement of infrared absorption and Raman scattering from molecules adsorbed at metal surfaces had already been observed (40,41); the initial theoretical treatment

$$S = 192\pi^2 c |E_\omega|^4 \left(\frac{2\omega R}{c} \right)^4 \left\{ \left| \frac{e[1 - \epsilon(2\omega)]/8\pi m \omega^2}{[\epsilon(\omega) + 2][\epsilon(2\omega) + 2]} \right|^2 + \frac{36}{5} \left| \frac{e[\epsilon(\omega) - 1]/8\pi m \omega^2}{[\epsilon(\omega) + 2]^2 [2\epsilon(2\omega) + 3]} \right|^2 \right\} \quad (5)$$

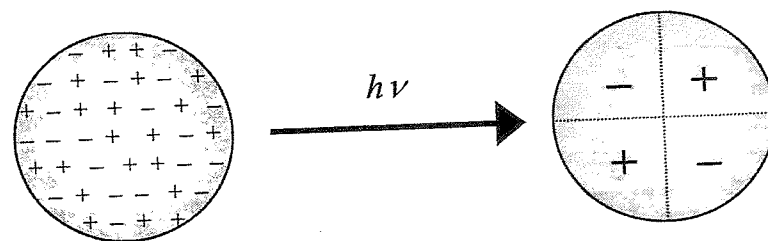
sought to explain such enhancement. Using a previously derived expression for the nonlinear polarization, and incorporating the familiar Mie solution for the local field at a spherical surface, the authors derived Eq. (5) for the total second-harmonic power, S , scattered by a small metal sphere (small compared with the wavelength of incident light). In the equation, m and e are the electron mass and charge, c is the speed of light, R is the sphere radius, E_ω is the incident intensity, and ϵ represents the dielectric constant of the material. The terms in brackets represent volume and surface contributions, respectively, to the scattered power. The authors further noted that (a) resonance enhancement is expected when $\text{Re}(\epsilon(\omega)) + 2 \approx 0$ (as in standard Mie theory); (b) near resonance, the surface contribution

Nonlinear Optical Properties

($[\epsilon(\omega) + 2]^{-4}$ dependence) is expected to dominate over the volume contribution ($[\epsilon(\omega) + 2]^{-2}$ dependence); (c) a two-photon resonance effect should also exist; and (d) all contributions should scale as the particle radius to the sixth power. Point (d) could also be expressed as a scaling of intensity with the square of the total number of atoms in the particle. For comparison, a log-log plot of the raw data (total β^2 versus particle radius) comprising the admittedly small experimental sample in Fig. 1 yields a slope of ~ 4.4 , corresponding to an apparent increase in HRS signal intensity as total number of atoms per particle to the ca. 1.5 power, or roughly the square of the number of surface atoms per particle. Clearly, additional experimental work would be valuable.

Recalling the linear scaling of plasmon absorption intensity with number of atoms per particle (at least for smaller particles), the Agarwal-Jha theory also implies that HRS signals will scale as the square of the plasmon absorption coefficient or oscillator strength. The raw data comprising Fig. 1 suggest a scaling of HRS signal intensity as plasmon extinction coefficient to the power of ~ 1.5 . (Interestingly, the corresponding theory for molecular chromophores predicts—based of course on different physics—a scaling with oscillator strength to the fourth power [see Eq. (4), where HRS signal intensity is proportional to β^2].)

Agarwal and Jha's work was later refined and extended by Hua and Gersten (42), who used a perturbation theory approach and a full Mie theory derivation to arrive at an analytical expression for an effective cross section for second-harmonic generation. Their results explicitly showed the importance of higher-mode (i.e., quadrupolar) contributions to the nonlinear scattering. [Note, however, that the second term in Eq. (5)—the "surface" term—is in fact a quadrupolar scattering term.] Scheme 1 illustrates in a qualitative way the idea of quadrupolar polarization of a small metallic sphere by incident electromagnetic radiation. Notably, quadrupolar second-harmonic generation is not subject to the noncentrosymmetry constraint associated with most dipolar SHG mechanisms. For very small particles, the Hua-Gersten theory—like the Agarwal-Jha theory—predicts a



Scheme 1 Qualitative depiction of quadrupolar polarization of a metal sphere. Note the loss of centrosymmetry upon quadrupolar polarization.

radius-to-the-sixth-power (or number of atoms to the second power) dependence for the per-particle nonlinear scattering intensity. As the particle size increases, however, the sensitivity to size is predicted to weaken, ultimately dropping to a radius (r)-to-the-fourth-power dependence. Additionally, the shift toward r^4 dependence is predicted to occur more readily under near-resonance conditions. [Interestingly, the effect is paralleled by a shift from radius-cubed to radius-squared for the particle-size dependence of the linear absorption component of the plasmon extinction coefficient (25,42).] Preliminary modeling studies by Hua and Gersten for aluminum and silver nanoparticles (5–20 nm) showed multiple peaks in the calculated SHG cross section excitation profile corresponding to dipolar and quadrupolar plasmon resonance frequencies.

Recently, Dadap and co-workers treated the case of HRS from small spherical particles (43). Their theory emphasizes the role of the particle surface in creating the nonlinear response; presumably the theory, if further developed, will be useful in describing or predicting the nonlinear spectroscopic consequences (beyond simple dielectric medium effects) of specific particle surface modifications. Like Agarwal and Jha and Gersten and Hua, these workers note the importance of higher-order multipole effects and cite contributions from nonlocal dipole moment excitation and from local quadrupole moment excitation as the main contributors to the second-order signal. Interestingly, the Dadap treatment is not limited to metals, although sample calculations for aluminum particles were presented. From the sample calculations, they conclude that resonance enhancement should occur at excitation energies equaling $E(\text{plasmon}) \cdot (3)^{-1/2}$, $E(\text{plasmon}) \cdot (10)^{-1/2}$, $E(\text{plasmon}) \cdot (12)^{-1/2}$, and $E(\text{plasmon}) \cdot (2/5)^{+1/2}$. Like the earlier theories, the treatment of Dadap and co-workers predicts a limiting radius-to-the-sixth-power dependence for the per-particle HRS intensity. In addition, the theory treats second-harmonic radiation patterns as well as polarization effects, where the former apparently have yet to be explored experimentally. The authors state that the latter can be used to distinguish nonlocal dipole scattering contributions from quadrupolar contributions to the overall nonlinear response.

As new experimental findings emerge, corresponding needs and opportunities for further theory development will emerge. Some of the simpler existing experimental observations that a complete theory could help to explain are

1. The strong sensitivity of incoherent second-order nonlinear scattering responses to small-aggregate formation
2. An apparent scaling of near-resonant single-particle NLO signal intensity neither with particle area nor particle volume, but with a stronger function of particle size
3. The sensitivity of particle-cluster-based HRS signals to precise cluster symmetry and particle-particle separation distance
4. The existence of nonunit depolarization ratios

We note that to some extent available theories already are capable of accounting for observations 2 and 4.

IX. APPLICATIONS

The notably different NLO responses for isolated versus aggregated metal nanoparticles, together with the comparative enormity of the responses, opens the door to many potential applications. The well-known red-to-blue color change of gold nanoparticles upon aggregation has been exploited in a sensitive colorimetric DNA sensing method, which uses oligonucleotide-coated nanoparticles designed to aggregate in the presence of a specific DNA base sequence (44). Accurate sensing of specific DNA sequences has clear technological potential for rapid disease screening. Vance and co-workers (45,46) have shown that similar sensing can be achieved with HRS as the reporter. The difference is that formation of very small aggregates (too small to induce a significant change in the linear extinction spectrum) can be detected. Under identical experimental conditions, the switch from linear to nonlinear solution-phase detection extends the DNA detection limit by a little less than an order of magnitude.

An important characteristic of the gold particle-based DNA detection system is the “melting” transition of the complementary DNA strands. In the presence of the correct complementary strand, the particles are linked. At sufficiently high temperatures enough of the hydrogen bonds connecting the strands are broken to unzip the oligonucleotides, “melting” the DNA and releasing the particles (44). Above the melting temperature, little HRS is observed. Below this temperature, substantial signals are seen. One application of the HRS detection scheme has been to evaluate the DNA concentration dependence of the “melting” temperature. Consistent with the underlying thermodynamic description, the “melting” temperature decreases as the concentration is lowered. In principle, the temperature dependence should provide qualitative or semiquantitative information about the corresponding enthalpy of complementary strand association/dissociation.

As noted earlier, modification of gold nanoparticles with alkanethiols and other surface passivating groups is straightforward and well documented. This allows for rational design of particles with specific surface properties. A potential practical application of such design is a sensitive technique for detecting toxic heavy metals in water. By decorating the surfaces of gold nanoparticles with 11-mercaptoundecanoic acid [$\text{HS}-(\text{CH}_2)_{10}-\text{CO}_2\text{H}$; MUA], the particles become efficient metal detectors in solution (32). The terminal acid functionality chelates certain divalent metal ions, including Pb^{2+} , Cd^{2+} , and Hg^{2+} —thereby inducing particle aggregation (shown schematically in Fig. 6.) Again, HRS is sensitive to this aggregation, and substantial HRS signal enhancement from 13-nm gold particles coated with MUA is seen in the presence of very small amounts of lead or

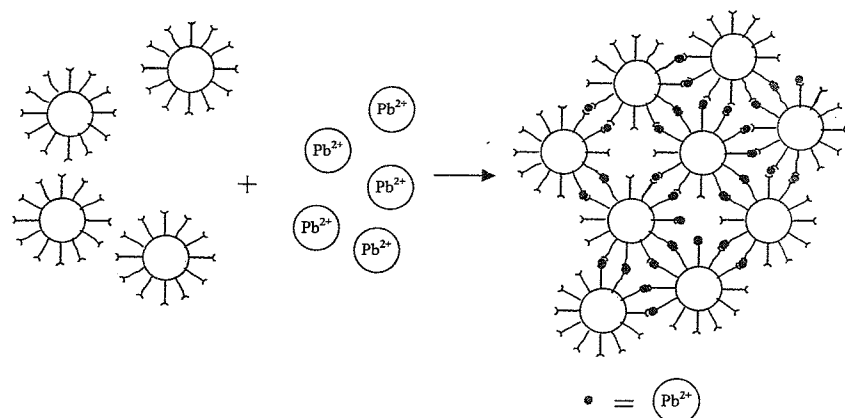


Fig. 6. Schematic representation (not drawn to scale) of metal-ion-induced aggregation of gold nanoparticles. The MUA(—)-decorated gold particles shown on the left are aggregated in the presence of Pb^{2+} in solution; the nonlinear (HRS) response of the resulting aggregates (shown on the right) is nearly an order of magnitude greater than that of the unlinked particles. Note that in this case Hg^{2+} and Cd^{2+} will also induce the aggregation and lead to signal enhancement.

cadmium. Addition of ethylenediaminetetraacetic acid—an extremely effective metal ion extraction agent—largely reverses the response. No enhancement is seen upon addition of zinc ions, consistent with the known poor affinity of Zn^{2+} for carboxylate ligands. Judicious tuning of the metal particle size and the receptor ligand's surface concentration could substantially increase analytical sensitivity, while manipulation of the ligand's chemical composition could enhance selectivity.

Finally, the enormous nonlinear scattering coefficients for metal nanoparticles featuring visible-region plasmon bands suggests that they could prove particularly useful in photonics applications. In contrast to metal macrostructures, the particles are characterized by good red and near-IR transparency, an important prerequisite in photonic devices because of the need to avoid absorption losses. Nevertheless, there are some obvious technical challenges in meaningfully utilizing metal nanoparticles as nonlinear optical components in photonic devices. One is to align or otherwise configure the particles so that efficient *coherent* SHG can be accomplished. [Recall that with HRS (incoherent SHG) individual particle responses largely cancel each other.] A related challenge will be to achieve the needed configuration without compromising red and near-IR transparency; recall

that placement of particles in close proximity to each other typically leads to plasmon-enhanced red and near-IR region scattering and higher multipole absorption.

ACKNOWLEDGMENTS

We thank the MURI Program of the Army Research Office for financial support of this research through grant no. DAAG55-97-1-0133.

REFERENCES

1. PN Prasad, DJ Williams. *Introduction to Nonlinear Optical Effects in Molecules and Polymers*. New York: Wiley, 1991.
2. E Hendrickx, K Clays, A Persoons. *Acc Chem Res* 31:675–683, 1998.
3. A Willetts, JE Rice, DM Burland, DP Shelton. *J Chem Phys* 97:7590–7599, 1992.
4. P Kaatz, EA Donley, DP Shelton. *J Chem Phys* 108:849–856, 1998.
5. JA Giordmaine. *Phys Rev* 138:A1599–A1603, 1965.
6. H Wang, ECY Yan, E Borguet, KB Eisenthal. *Chem Phys Lett* 259:15–20, 1996.
7. RM Corn, DA Higgins. *Chem Rev* 94:107–125, 1994 and references therein.
8. RW Terhune, PD Maker, CM Savage. *Phys Rev Lett* 14:681–684, 1965.
9. K Clays, A Persoons. *Phys Rev Lett* 66:2980–2983, 1991.
10. K Clays, A Persoons. *Rev Sci Instrum* 63:3285–3289, 1992.
11. K Clays, A Persoons. *Rev Sci Instrum* 65:2190–2194, 1994.
12. M Kauranen, A Persoons. *J Chem Phys*, 104:3445–3456, 1996.
13. P Kaatz, DP Shelton. *J Chem Phys* 105:3918–3929, 1996.
14. JL Oudar, DS Chemla. *J Chem Phys* 66:2664–2668, 1977.
15. FW Vance, BI Lemon, JT Hupp. *J Phys Chem B*. 102:10091–10093, 1998.
16. L Karki, FW Vance, JT Hupp, SM LeCours, MJ Therien. *J Am Chem Soc* 120: 2606–2611, 1998.
17. P Galletto, PF Brevet, HH Girault, R. Antoine, M. Broyer. *Chem Commun* 1999: 581–582.
18. R Antoine, PF Brevet, HH Girault, D. Bethell, DJ Schiffrin. *Chem Commun* 1997: 1901–1902.
19. R Antoine, M Pellarin, B Palpant, M Broyer, B Prével, P Galletto, PF Brevet, HH Girault. *J Appl Phys* 84:4532–4536, 1998.
20. K Clays, E Hendrickx, M Triest, A. Persoons. *J Mol Liq* 67:133–155, 1995.
21. M. Triest. Ph.D. thesis, Katholieke Universiteit Leuven, Belgium, 1994
22. J Li, RC Johnson, JT Hupp. Unpublished work.
23. P Galletto, PF Brevet, HH Girault, R Antoine, M. Broyer. *J Phys Chem B* 103: 8706–8710, 1999.
24. CG Blanchard, JR Campbell, JA Creighton. *Surf. Sci.* 120:435–455, 1982.
25. KL Kelly, TR Jensen, AA Lazarides, GC Schatz, Chapter 4 this volume, and references therein.

26. BMI van der Zande, MR Böhmer, LGJ Fokkink, C Shönenberger. *J Phys Chem B*. 101:852–854, 1997.
27. CA Foss, MJ Tierney, CR Martun. *J Phys Chem* 96:9001–9007, 1992.
28. ML Sandrock, CD Pibel, FM Geiger, CA Foss, Jr. *J Phys Chem B* 103: 2668–2673, 1999.
29. WH Yang, J Hulteen, GC Schatz, RP VanDuyne. *J Chem Phys* 104:4313–4323, 1996.
30. Y Liu, JI Dadap, D Zimdars, KB Eisenthal. *J Phys Chem B* 103:2480–2486, 1999.
31. For example, LM Liz-Marzán, M Giersig, P Mulvaney. *Langmuir* 12:4329–4335, 1996.
32. RJ Johnson, Y Kim, JT Hupp. Unpublished studies.
33. FW Vance, BI Lemon, JA Ekhoft, JT Hupp. *J Phys Chem B* 102:1845–1888, 1998.
34. LC Brousseau III, JP Novak, SM Marinakos, DL Feldheim. *Adv Mater* 11:447–449, 1999.
35. FW Vance, JP Novak, RC Johnson, JT Hupp, DL Feldheim. BI Lemon, LC Brousseau. *J Am Chem Soc* 122:12029–12030, 2000.
36. T Verbiest, K Clays, A Persoons, F Meyers, JL Bredas. *Opt Lett* 18:525–527, 1993.
37. CP Collier, RJ Saykally, JJ Shiang, SE Henrichs, JR Heath. *Science* 277:1978–1981, 1997.
38. Remacle F, Collier CP, Markovich G, Heath JR, Banin U, Levine RD. *J Phys Chem B*. 102:7727–7734, 1998.
39. GS Agarwal, SS Jha. *Sol State Commun* 41:499–501, 1982.
40. A Harstein, JR Kirtley, JC Tsang. *Phys Rev Lett* 45:201–204, 1980.
41. PN Sanda, JM Warlaumont, JE Demuth, JC Tsang, K. Christmann, JA Bradley. *Phys Rev Lett* 45:1519–1523, 1980.
42. XM Hua, JI Gersten. *Phys Rev B* 33:3756–3764, 1986.
43. JI Dadap, J Shan, KB Eisenthal, TF Heinz. *Phys Rev Lett* 83:4045–4048, 1999.
44. RA Reynolds, CA Mirkin, RL Letsinger. *J Am Chem Soc* 122:3795–3796, 2000.
45. FW Vance. Ph.D. thesis, Dept. of Chemistry, Northwestern University, 1999.
46. FW Vance, J. Storhoff, JT Hupp, CA Mirkin. Unpublished studies.